

The suitability of different vegetation indices to analyses area with landslide propensity using Sentinel -2 Image

Lucilia do Carmo Giordano¹ - ORCID: 0000-0002-1302-6694

Mara Lúcia Marques² - ORCID: 0000-0002-1478-565X

Fábio Augusto Gomes Vieira Reis³ - ORCID: 0000-0003-3918-6861

Claudia Vanessa dos Santos Corrêa¹ - ORCID: 0000-0003-2524-8443

Paulina Setti Riedel¹ - ORCID: 0000-0002-5879-9762

¹ Universidade Estadual Paulista (UNESP), IGCE-UNESPetro Cento de Ciências Naturais Aplicadas, Rio Claro - SP, Brasil.

E-mail: lucilia.giordano@unesp.br; claudia.correa@unesp.br; paulina.riedel@unesp.br

²Pontifícia Universidade de Campinas, Escola de Arquitetura, Artes e Design, Campinas -SP, Brasil.

E-mail: mara.marques@puc-campinas.edu.br

³Universidade Estadual Paulista (UNESP), IGCE- Departamento de Geologia, Rio Claro - SP, Brasil.

E-mail: fabio.reis@unesp.br

Received in 28th February 2023.

Accepted in 23th September 2023.

Abstract:

Vegetation Indices (VIs) provide spatial information on the vegetation state, which has been associated with landslide propensity. To evaluate how VIs information indicate the landslide propensity, the current study analyzed nine different IVs to identify the categories of vegetation states in the hydrographic basin of Pedra Branca before and after landslide event. The different VIs were obtained using Sentinel-2A (2016) and Sentinel-2B (2018) images. All VIs were tested by cross-table analysis regard to the ability to identify the calculated area for landslide scars, and the VIs were also compared to the NDVI reference by error matrix for the analysis of the accuracy in identifying the vegetation state before the landslide occurrence. The areas with landslide scars totalized 86700m² in 2018 image and NDVI matched ~57% of the No Vegetation category. Before the landslide event, almost all VIs indicated a loss of vegetation vigor (with exception of RENDVI and ARVI) in 2016 image. In addition, the indices (exceptionality MSI) also presented high rates of match to the analysis of NDVI in discerning both Intermediate and Vigorous Vegetation states. However, the areas presenting a healthy vegetation state are reduced, which therefore might be indicating the propensity to landslide event before their occurrences.

Keywords: Vegetation; Landslide scars; Digital image processing; Remote Sensing.

How to cite this article: GIORDANO LC, MARQUES ML, REIS FAGV, CORRÊA CVS, RIEDEL OS. The suitability of different vegetation indices to analyses area with landslide propensity using Sentinel -2 Image. *Bulletin of Geodetic Sciences*. 29(3): e2023008, 2023.



This content is licensed under a Creative Commons Attribution 4.0 International License.

1. Introduction

Landslides are considered the main natural process of gravitational mass. In geomorphology, are described as the movement of a mass of rock, debris, or earth down a slope, under the influence of gravity and are triggered by intense rainfall events (Guidicini and Nieble 1984, Wolle and Carvalho 1989, Zhang et al. 2014, Segoni et al. 2018).

Hillslope and vegetation cover mapping might indicate the propensity to landslide. Vegetation Indices (VI) obtained by remote sensing products provide spatial and temporal information about the condition and abundance of vegetation cover, enabling the analysis to determine its health and stress, types of soil cover, and its disturbances (Durante et al. 2014, Schiavo 2016).

The lack of vegetation might trigger landslide in the escarpment, and large vegetation cover can reduce landslide propensity. Vegetation indices might be applied as a procedure to evaluate landslide propensity through its ability to distinguish the different states of vegetation on the surface (Dahigamuwa et al. 2016, Yi et al. 2019), and considering the role of the vegetation cover on hillslope stability (Schwarz et al. 2010), as well as the potential of the state and the characteristics of vegetation to integrate with other causative factors (e.g., climatology, topography, land use and hydrogeology) to improve the identification of landslide susceptibility in a given area (Gomes, et al. 2020, Abey Siriwardana and Gomes 2022).

The VI is a metric of vegetation state, but there are different assessments of VI, all produced by the combination of spectral bands from remote sensing images (Rouse et al. 1973, Salas and Henebry 2014, Hu et al. 2022). The spectral bands record the electromagnetic irradiance of different objects covering the earth's surface in the following wavelengths: visible (400–700nm), near-infrared – NIR (700–1300nm), shortwave infrared – SWIR (1300–2500nm). Through the irradiance responses, the components determining the VI are: (i) photosynthetic pigments (chlorophylls and carotenoids) of healthy green leaves, through the absorption of energy in the Green (400–500nm) and Red (600–700nm) (Gitelson and Merzlyak 1998); (ii) cellular structure of healthy leaves promotes the spectral spread and refraction discontinuity in the spongy mesophyll in the NIR; and (iii) leaf water content influences vegetation reflectance in SWIR, with low reflectance characterizing water absorption by vegetation at 1400 and 1940nm and increase in reflectance at wavelength $1400\text{nm} < \lambda < 1900\text{nm}$ characterizing radiation absorption by atmospheric water vapor (Daughtry et al. 2000, Prabhakar et al. 2012).

In fact, the vigor and productivity of the vegetation are factors under influence of leaf chlorophyll, canopy water, and nitrogen contents in soil, which are also assessed by the radiation absorbed between the lengths of 400 to 700nm, hence determining the state of the photosynthesis process (Finch et al. 2004). In this way, it was stated that chemical and morphological information of the plants are related to the spectral reflectance of remote sensing products, taking into account that the leaves are among the elements of vegetation which most contribute to the signal detected by the optical sensors, as a function of their three tissues composition – epidermis, photosynthetic mesophyll (palisade parenchyma and spongy mesophyll) and vascular tissue (Colwell 1974, Vogelmann 1993, Noda et al. 2021).

Among the VIs, it might highlighted the Normalized Vegetation Index (NDVI), which uses the Red and NIR bands, and the values derived from the NDVI, such as the ARVI (Atmospherically Resistant Vegetation Index), which uses reflectance measurements in the Blue wavelength to correct the atmospheric scattering effects recorded in the Red reflectance spectrum (Kaufman 1984, Kaufman and Tanre 1992), and the NDWI (Normalized Difference Water Index) used to discriminate vegetation according to the water content in the sheets based on NIR bands (Gao 1996, McFeeters 1996, Zhu et al. 2020).

There are also indexes influenced by the water content in the leaves, such as the MSI (Moisture Stress Index), which determines the ratio between the bands sensitive to leaf water changes (Rock et al. 1986, Hunt et al. 1987, Hunt and Rock 1989, Hunt 1991), and the NDII (Normalized Difference Infrared Index), which differentiates the

vegetation according to the water content in the canopy foliage by the normalized ratio of the NIR and Thermal Infrared bands (Hardisky et al. 1983, Hunt and Rock 1989).

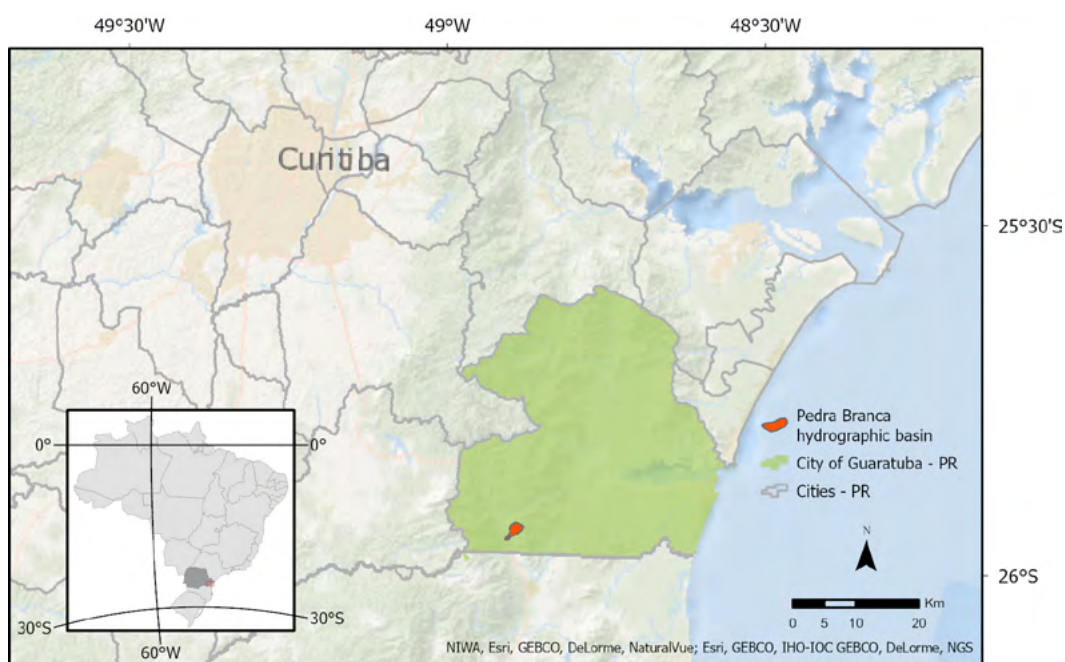
It should be noted, however, that a natural forest ecosystem is susceptible to different degradation processes and that, therefore, there is a need to obtain accurate data, as demonstrated when using Sentinel-2 images to determine the NDVI for the evaluation of the Mediterranean natural forest integrity inside conservation areas (Recanatesi et al. 2018) and the spatio-temporal vegetation patterns in Beijing–Tianjin–Hebei region (Zou et al. 2022).

However, there are no studies reporting the comparison between VIs regarding the potential to the analysis of vegetation states, which might be able to indicate changes in areas of natural vegetation cover before landslide events. Therefore, the current study aimed at the use Sentinel-2 images to determine different VIs and analyze the suitability of each VI in assessing the quality of vegetation states in areas before and post landslide occurrence.

2. Study Area

The present study was carried out in Pedra Branca hydrography basin, in the municipality of Guaratuba, Paraná State, Brazil (Figure 1). The average annual temperature is 21.09°C ranging from 17.26 to 25.14°C. In January, February, and March, the highest metric rainfall indexes are recorded, with an average annual rainfall of 1,959mm. The relative humidity is high, with average values fluctuating around 85% (Maack 1981). In the hillslopes areas are rocky outcrops associated with Leptosols soils, which also occur in the hills, Ferralsols, and Cambisols soils (EMBRAPA 1984).

According to the classification system of the Brazilian vegetation proposed by Veloso et al. (1991), the steepest mountain areas under dissected relief are occupied by the Unit of Dense Anthropophilic Forest Montana, characterized by species of the genus *Ocotea*, *Copaifera*, and *Pterocarpus*, with under forest occupy by epiphytes, pteridophytes, palmaces, and heliophyte fast-growing species. In the shallow Leptosols soils already intensely eroded and in rock outcrops, the herbaceous-graminoid cover predominates.



Source: IBGE (2015).

Figure 1: Location of the study area.

3. Material and Method

3.1 Material

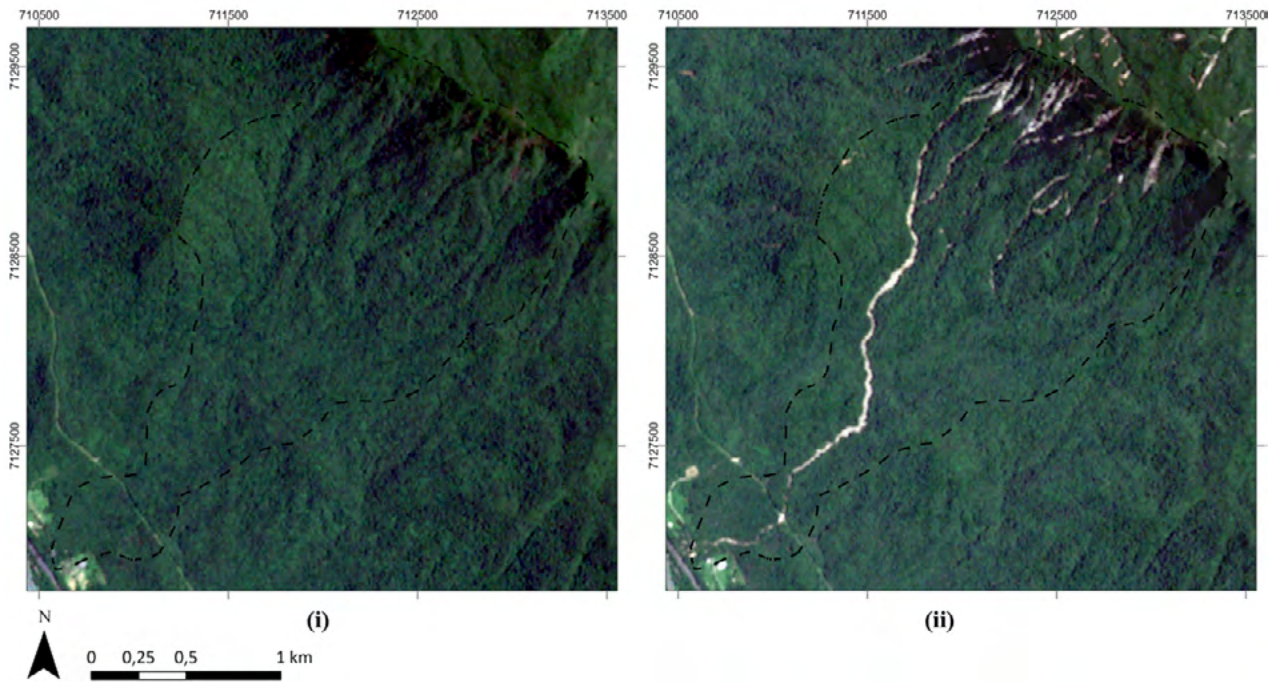
The Sentinel-2 images were obtained from the Global Monitoring for Environment and Security (GMES) Program of the European Space Agency (ESA 2018), with the purpose to contribute to monitoring the variability of land surface conditions and changes in vegetation cover (Debastiani et al. 2019), using Sentinel-2A images (acquisition date December 6, 2016, spatial resolution of 10m, exceptionality to B5, B6, B8A and B11 bands, which have 20m, solar angle of 67.98° and cloud cover 0%) and Sentinel-2B (acquisition date on January 5, 2018, spatial resolution of 10m, solar angle of 64.77° and cloud cover 0.61%). The Sentinel-2 images were acquired with Level-2A products providing the format Bottom-Of-Atmosphere (BOA) reflectance. Table 01 shows the distribution of wavelengths and spatial resolution of each of the 13 bands of Sentinel-2 sensors (A and B), used to produce vegetation index, with emphasis on the SWIR (Short Wavelength Infrared, i.e., shortwave infrared) region, and also to the region called Red Edge, the region between 680 and 750nm) where sudden changes in leaf reflectance are detected and, therefore, used to detail the information about vegetation (Horler et al. 1983). Figure 2 (Panels i and ii) depicts the Sentinel-2A and 2B images used for the analysis of vegetation states before and post landslide event with scars defined.

Table 1: Key characteristics of Sentinel-2A and 2B from the Multispectral Imaging Mission (MIS).

| Spectral Band | Resolution Spatial (m) | Sentinel - 2A* | Sentinel - 2B* |
|--------------------|------------------------|-------------------------|-------------------------|
| | | Central wavelength (nm) | Central wavelength (nm) |
| B2 (Blue) | 10 | 496.6 | 492.1 |
| B3 (Green) | | 560.0 | 559.0 |
| B4 (Red) | | 664.5 | 665.0 |
| B8 (Near Infrared) | | 835.1 | 833.0 |
| B5 (Red Edge1) | 20 | 703.9 | 703.8 |
| B6 (Red Edge2) | | 740.2 | 739.1 |
| B7 (Red Edge3) | | 782.5 | 779.7 |
| B8A (Red Edge4) | | 864.8 | 864.0 |
| B11 (SWIR1) | 60 | 1613.7 | 1610.4 |
| B12 (SWIR2) | | 2202.4 | 2185.7 |
| B1 (Aerosol) | | 443.9 | 442.3 |
| B9 (Water vapor) | | 945.0 | 943.2 |
| B10 (Cirrus) | | 1373.5 | 1376.9 |

* Obs. The Sentinel 2A and B images were applied respectively to the analyses of vegetation state in 2016 and 2018 dates.

Source: Vanhellemont and Ruddick (2016).



Source: European Space Agency’s Global Monitoring for Environment and Security (GMES) Programmer (ESA 2018).

Figure 2: (i) Sentinel-2A images (December 6, 2016) and (ii) Sentinel-2B (January 5, 2018).

3.2 Procedures

The method approached in the present study establishes the exploratory mapping of the data obtained by digital processing of remote sensing images, using different VI algorithms to analyze of the vegetation state and the landslide occurrence (Figure 3).

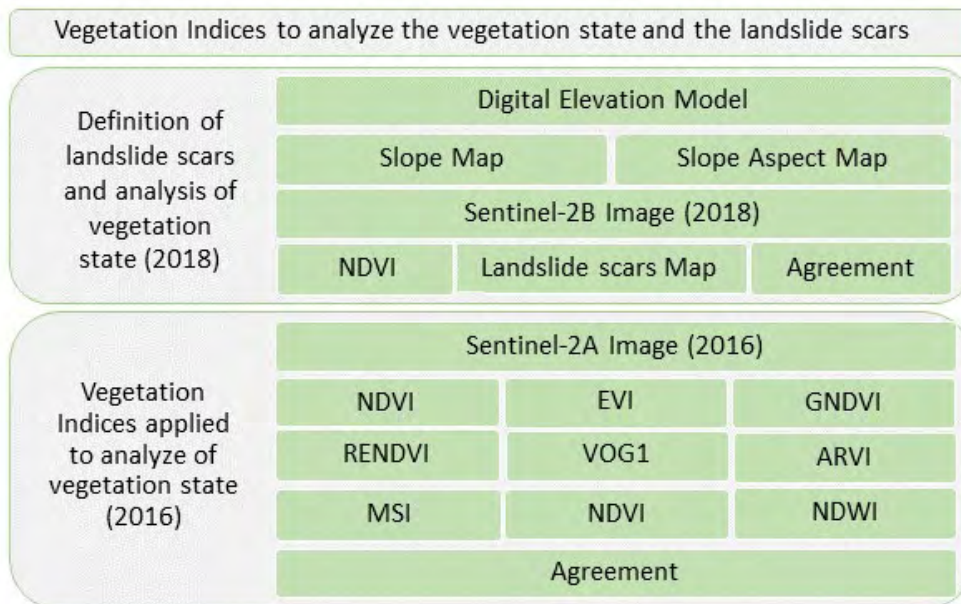


Figure 3: Flowchart for the analytic procedures.

The slope and slope aspect mapping were produced (Figures 4 and 5). These mappings were elaborated from the digital elevation model (DEM) generated by the interpolation of the contour lines from IBGE Topographic Chart 1:50,000, which have equidistance of 20m, and using the “Topo to Raster” tool in the ArcGIS program (ESRI 2015). This DEM is appropriated to characterize the relief, since it was generated with high spatial resolution and the area is located on a physiographic compartment without human interference.

The identification and mapping of the landslide scars used the Sentinel-2B (2018) image. The procedures involved the vectorization of the features based on visual interpretation. Afterward, DEM supported the definition of the landslide scars by considering the profile of the relief, as the slope of the area and the orientation of the hillside (Zhang et al. 2014). All mapped landslide scars were located in gradients above 22°, highlighting the occurrence of slopes higher than 32° upstream of the watersheds. It is also noteworthy that despite the predominance of hillsides oriented to the South, Southeast, and Southwest at the upper boundary of the basin, most of the landslide scars have occurred in the southwest-oriented hillside.

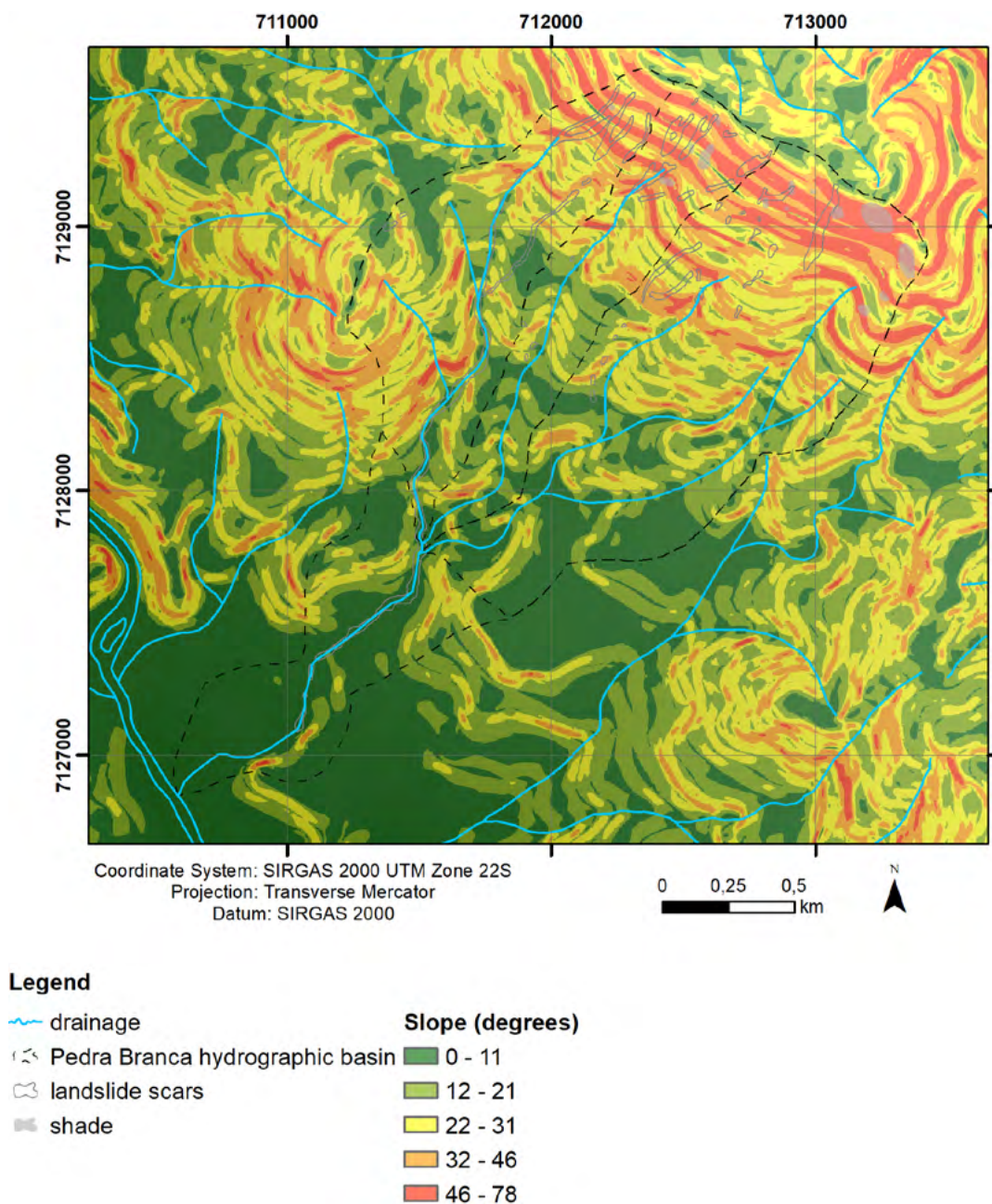


Figure 4: Slope gradients in Relief Map.

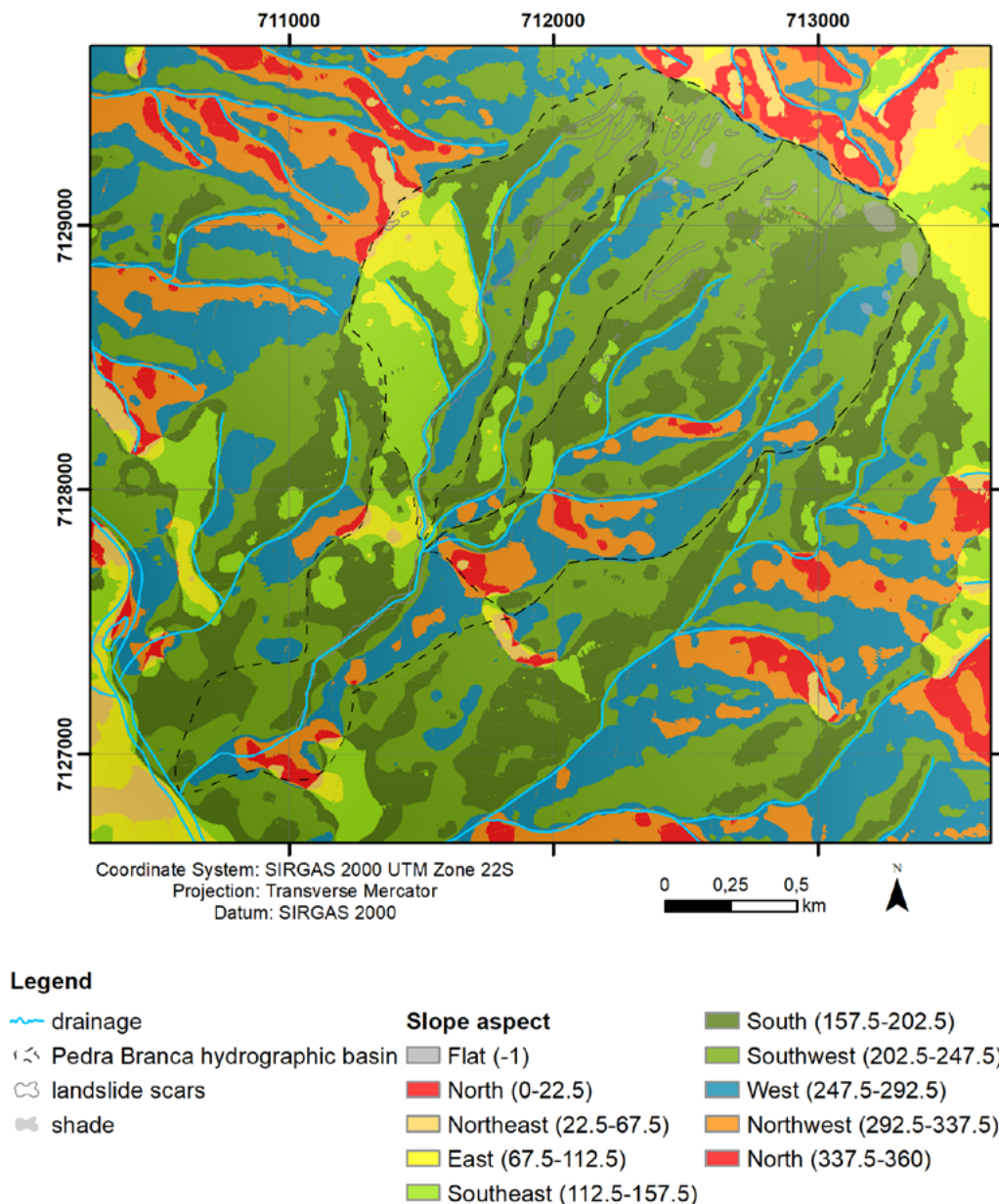


Figure 5: Slope Aspect Map.

The Sentinel-2A image (2016) processing was performed in ArcGIS geographic information system (ESRI 2015), by applying the “Map Algebra” tool for the assessment of the NDVI, EVI, GNDVI, RENDVI, VOG1, ARVI, MSI, NDII, NDWI. When the assessment of the VI required the combination of bands with different spatial resolutions, the procedures considered normalizing for the low resolution (20m). For the Sentinel-2B image (2018) only NDVI was assessed. The sequence of the Vegetation Indices produced is as follows:

1. NDVI – Normalized Difference Vegetation Index according to Equation (1), with index variation between -1 to 1, and negative values corresponding to water, values close to zero (-0.1 to 0.1) (Rouse et al. 1973).

$$NDVI = \frac{(B8 - B4)}{(B8 + B4)} \quad (1)$$

2. EVI – Enhanced Vegetation Index according to Equation (2) which was developed from the NDVI index by optimizing the signal in dense canopy areas, where the leaf area index (LAI) is high, using the reflectance in blue wavelength. The information in this part of the spectrum can help correct soil signals and atmospheric influences, including aerosol, obtaining an index between -1 and 1, where healthy vegetation has values

ranging from 0.20 to 0.80 (Huete et al. 2002).

$$EVI = G * \frac{(B8 - B4)}{(B8 + C1 * B4 - C2 * B2) + L} \quad (2)$$

where $C1$ is the correction coefficient of atmospheric effects for the red band = 6, $C2$ is the coefficient of correction of atmospheric effects for the blue band = 7.5, L is the correction factor for soil interference = 1 and G is the gain factor = 2.5.

3. GNDVI – Green Normalized Difference Vegetation Index according to Equation (3) uses the reflectance of the Green spectrum, being more sensitive to chlorophyll concentration than NDVI (Gitelson et al. 1996).

$$GNDVI = \frac{(B8 - B3)}{(B8 + B3)} \quad (3)$$

4. RENDVI – Red Edge Normalized Difference Vegetation Index according to Equation (4) with index variation between -1 to 1, it employs measurements of reflectance along the spectral range called Red Border (705–750nm) (Sims and Gamon 2002).

$$RENDVI = \frac{(B6 - B5)}{(B6 + B5)} \quad (4)$$

5. VOG1 – Vogelmann Red Edge according to Equation (5) is an index sensitive to the combined effects of chlorophyll concentration on canopy foliage and its water content (722–742nm), obtaining index values between 0 and 20 (Vogelmann et al. 1993).

$$VOG1 = \frac{(B6)}{(B5)} \quad (5)$$

6. ARVI – Atmospherically Resistant Vegetation Index according to Equation (6), with an index between -1 and 1 (Fan et al. 2015).

$$ARVI = \frac{B8 - (B4 - y * (B4 - b2))}{(8 + (B4 - y * (B2 - B2)))} \quad (6)$$

where $y=0.106$ (atmospheric correction constant).

7. MSI – Moisture Stress Index according to Equation (7), characterized by being sensitivity to the changes of leaf water content and the index has values between 0 and 3, with high values indicating water stress (Hunt Jr and Rock 1989).

$$MSI = \frac{(B11)}{(B8)} \quad (7)$$

8. NDII – Normalized Difference Infrared Index according to Equation (8), differentiates the vegetation according to the water content in the canopy foliage, with index values between -1 to 1, and the healthy vegetation with values between 0.02 and 0.6 (Hardisky et al. 1983).

$$NDII = \frac{(B8 - B11)}{(B8 + B11)} \quad (8)$$

9. NDWI – Normalized Difference Water Index according to Equation (9), differs from the other indexes by employing the SWIR and Red Edge bands (Gao 1996).

$$NDWI = \frac{(B8A - B11)}{B8A + B11} \quad (9)$$

The thematic maps resulting from each Vegetation Indices were classified into four categories, according to the VI values: (1) red, areas with no vegetation; (2) orange, undergrowth or declining vegetation; (3) light green,

intermediate vegetation and (4) green, vigorous vegetation (Table 2). These categories were defined according to the recommendation of Rouse et al. (1973), which considered negative values as areas of rock, sand, and exposed soil, low but positive values representing shrubs and pastures (approximately 0.2 to 0.4), while high values indicate temperate tropical forests and tropical, values close to 1.

Table 2: Range of values considered to define the categories of vegetation state.

| VI | Categories | | | |
|-----------------|---------------|----------------------|-------------------------|---------------------|
| | No vegetation | Declining vegetation | Intermediate vegetation | Vigorous vegetation |
| NDVI (-1 – 1) | -0.46 – 0.46 | 0.47 – 0.65 | 0.65 – 0.72 | 0.73 – 0.92 |
| EVI (-1 – 1) | -0.46 – 0.46 | 0.47 – 0.65 | 0.65 – 0.72 | 0.73 – 0.92 |
| GNDVI (-1 – 1) | -0.46 – 0.46 | 0.47 – 0.65 | 0.65 – 0.72 | 0.73 – 0.92 |
| RENDVI (-1 – 1) | -0.46 – 0.46 | 0.47 – 0.65 | 0.65 – 0.72 | 0.73 – 0.92 |
| VOG1 (0 – 20) | 0.41 – 1.90 | 2.00 – 2.24 | 2.50 – 2.70 | 2.80 – 4.50 |
| ARVI (-1 – 1) | -0.46 – 0.46 | 0.47 – 0.65 | 0.65 – 0.72 | 0.73 – 0.92 |
| MSI (0 – 3) | 0.68 – 3.00 | 0.54 – 0.87 | 0.48 – 0.53 | 0.17 – 0.47 |
| NDII (-1 – 1) | -0.31 – 0.22 | 0.23 – 0.29 | 0.30 – 0.33 | 0.34 – 0.68 |
| NDWI (-1 – 1) | -0.31 – 0.22 | 0.23 – 0.29 | 0.30 – 0.33 | 0.34 – 0.68 |

3.3 Statistical Analysis

The observed landslide scars measured on Sentinel-2B (2018) image were compared to NDVI categories through crosstab spatial analysis. To verify the vegetation state before the landslide events, the VIs obtained on Sentinel-2A (2016) were also compared to the observed landslide scars areas by using crosstab spatial analysis. The accuracy of other VIs to match the information assessed with NDVI analysis on Sentinel-2A (2016) image was tested by calculating an error matrix to evaluate the accuracy among each category, using analytic spatial tools of ArcGIS (ESRI 2015).

4. Results and Discussion

The identification of areas with landslide scars is depicted in Figure 6 (Panel i), which was measured from landslide events observed on Sentinel-2B (2018) image, and totalized 86700m². When compared to the most used VI (NDVI) in Figure 5 (Panel ii), the total area identified as No Vegetation category matched only ~57%. The NDVI was considered the reference VI, as has been widely used for remote sensing of vegetation for many years (Gao 1996, Hu et al. 2022), particularly to map landslides post-failure damage to plant (Jacquemart and Tiampo 2021), since it was shown to be sensitive primarily to the green leaf area or green leaf biomass (Durante et al. 2014, Fan et al. 2015). However, the NDVI classified some parts of landslide scars areas as Declining (~36%) and Intermediate Vegetation (~7%), suggesting that some vegetation remained on the scars. In fact, the level of vegetation recovery has been reported to be uneven over time in bare deposits post landslide occurrence due to mountain earthquake events (Shen et al. 2020).

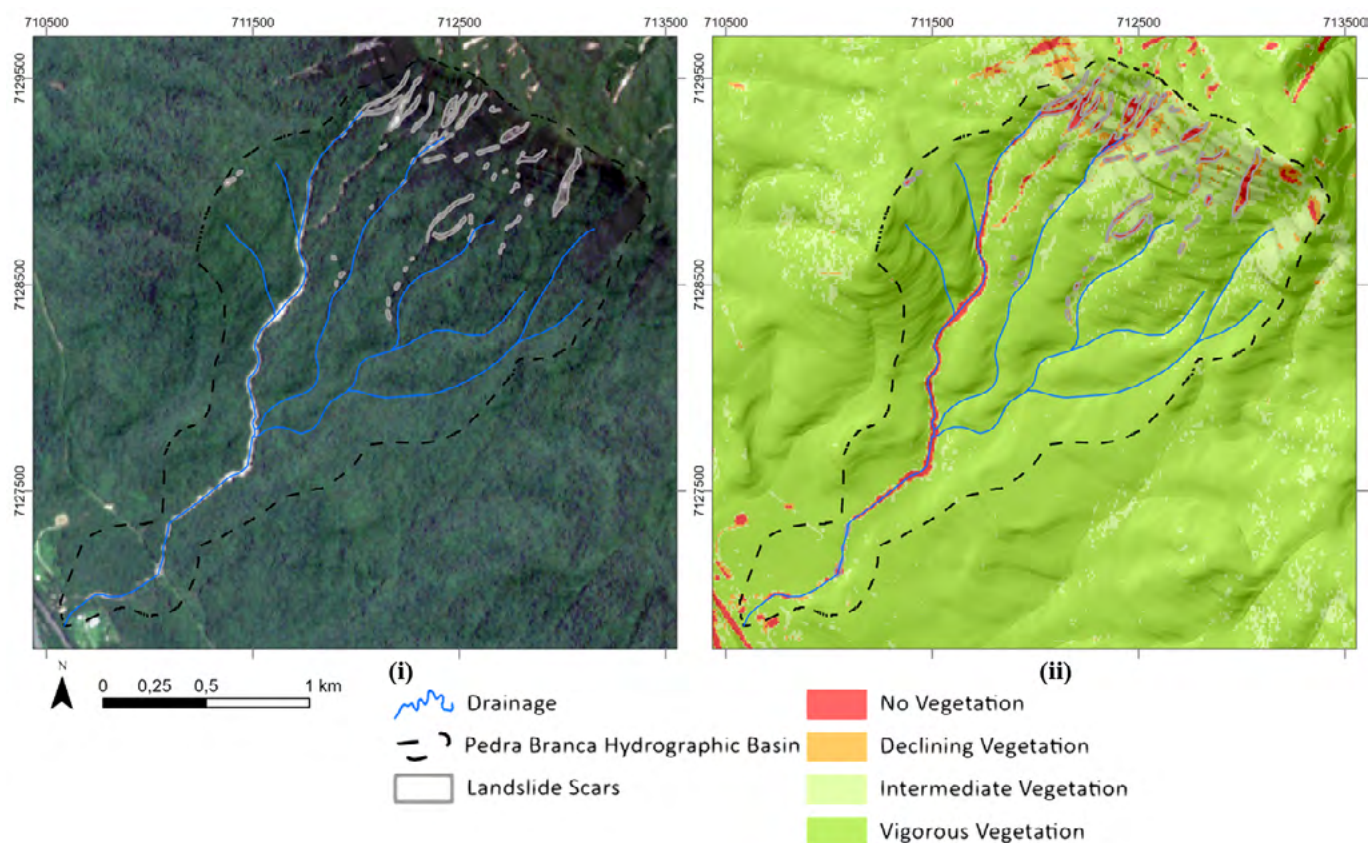


Figure 6: Identification of landslide scars through visual interpretation (Panel i) and categories of vegetation state from NDVI (Panel ii) on Sentinel-2B (2018).

The categories of vegetation state obtained to the different VIs in the areas where the landslide scars were observed can be seen in Table 3. With exception of RENDVI and ARVI, all of the others VIs indicated that the vegetation state was suggests loss of vegetation vigor before the landslide event in the areas which corresponding to landslide scars in 2018.

Table 3: Vegetation state according to different VIs in 2016 in the areas corresponding to landslide scars in 2018.

| Category | NDVI | EVI | GNDVI | RENDVI | VOG1 | ARVI | MSI | NDII | NDWI |
|-------------------------|------|-----|-------|--------|------|------|-----|------|------|
| No Vegetation | 11% | 0% | 0% | 1% | 0% | 0% | 18% | 4% | 2% |
| Declining Vegetation | 20% | 26% | 12% | 26% | 13% | 4% | 36% | 22% | 12% |
| Intermediate Vegetation | 39% | 65% | 58% | 30% | 53% | 8% | 34% | 72% | 56% |
| Vigorous Vegetation | 30% | 7% | 30% | 43% | 34% | 88% | 12% | 2% | 30% |

Figure 7 shows the results obtained for each VI. It can be observed that the category No Vegetation was not distinguished in the basin hydrographic area from EVI and ARVI, and the indices EVI, GNDVI, VOG1, and ARVI were not able to identify the category in the area corresponding to landslide scars, therefore compromising the identification of exposed soil and landslide scars due to past landslide events (Zhang et al. 2014). In turn, the category Declining Vegetation, which has the ability for representing the areas prone to landslide, tends to present high values for MSI, intermediate values for NDVI, EVI, and RENDVI, and low values for ARVI, GNDVI, VOG1, and NDWI (Table 3). Independently of this variation of values, the trends of reduced vegetation health were recognized for five of the nine VIs analyzed, which might indicate the need to monitor this area more often, as suggested by Jacquemart and Tiampo (2021) after demonstrating that a decrease in vegetation productivity or coverage is often observed in area ongoing a landslide event.

In addition, the categories corresponding to Intermediate and Vigorous Vegetation presented values (respectively) to medium-to-high and medium-to-low in the areas corresponding to landslide scars, with the exception to ARVI (Table 3). On the other hand, the healthy state of vegetation was considered satisfactory just for a minor part of the area corresponding to landslide scars. These results indicate that the vegetation cover was degrading in the area corresponding to landslide scars in 2018, and hence also providing important information regarding the risk of landslide in the future, as this profile was similar to those reported by Shen et al. (2020) and Jacquemart and Tiampo (2021).

It is also possible to observe from Figure 6, in association with the physical characteristics of the area (Figures 3 and 4), the prevalence of the categories No Vegetation and in Declining Vegetation in the Northeast part of the basin, where the slopes with a high degree are located. This observation is aligned with the evidence of an association between the slope and the landslide event (Karsli et al. 2009, Dahigamuwa et al. 2016). Despite this association has been recognized, studies report that hillsides facing the southwest, south, and southeast areas have highest tendency to vegetation recovery when compared to the hillside facing the north areas, therefore indicating that the orientation of the slopes influences the development of vegetation before and after the landslide event (Corrêa and Francelino 2015).

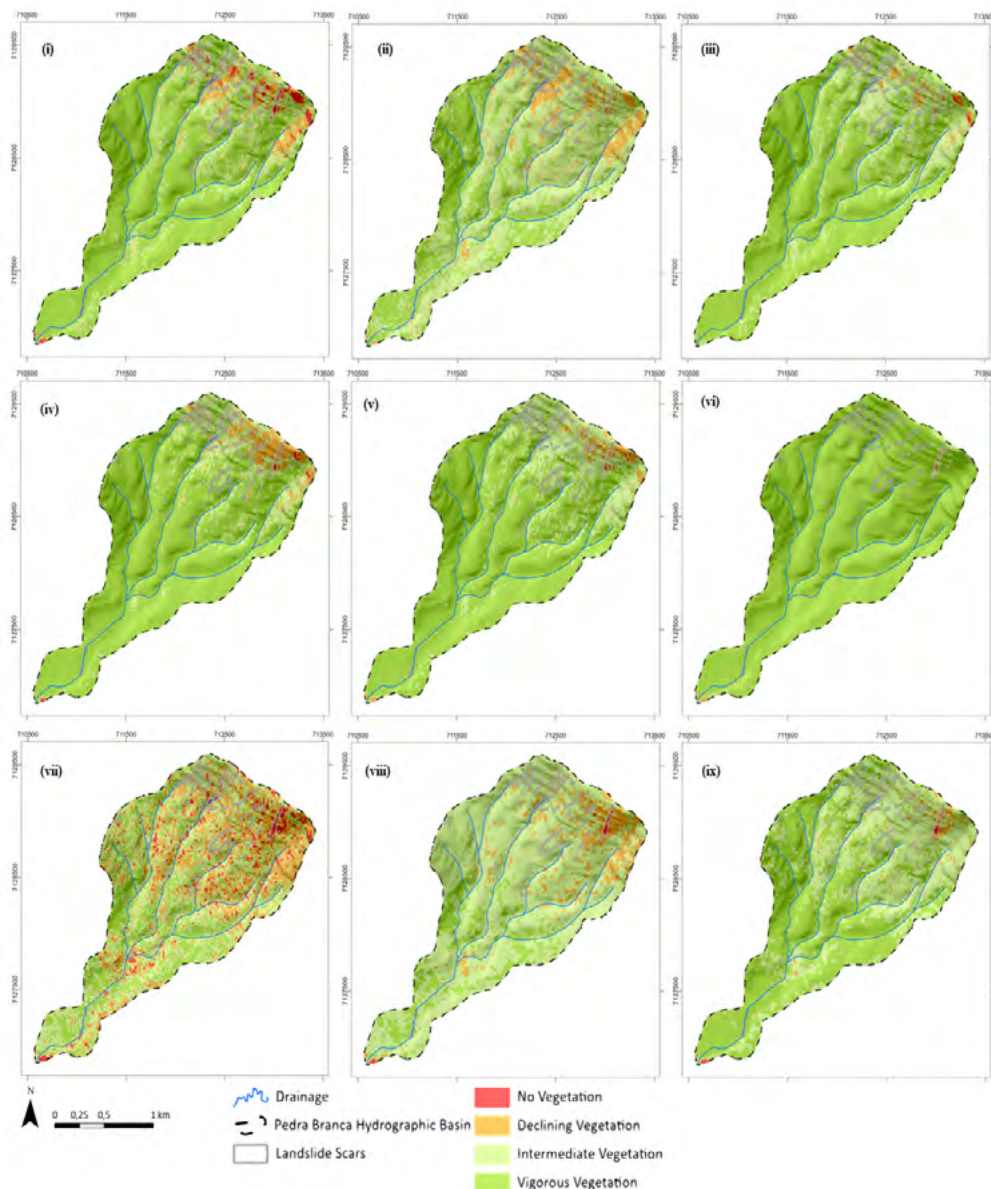


Figure 7: Thematic maps generated by the VIs on Sentinel-2A (2016) image: NDVI (i), EVI (ii), GNDVI (iii), RENDVI (iv), VOG1 (v), ARVI (vi), MSI (vii), NDII (viii) and NDWI (ix).

Table 4 shows the comparison between the VIs regarding the rate of correct matches to identify the vegetation categories in agreement with the reference analysis from NDVI on the Sentinel-2A (2016) image. The potential of the NDVI in providing detailed information about the health status of vegetation cover in preservation areas, as well as for the identification of areas with landslide propensity has been evidenced in the literature (Dahigamuwa et al. 2016, Recanatesi et al. 2018, Zou et al. 2022, Meena et al. 2022).

The highest rates of matches for the categories No Vegetation and Declining Vegetation were observed between NDVI with EVI and MSI, whereas almost all the indices (exceptionality MSI) presented high rates of matches to the analysis of NDVI in discerning both Intermediate and Vigorous Vegetation states. This finding enables to state that these VIs are not in agreement concerning the diagnostic of landslide propensity given to the reduced health status of the vegetation cover. However, landslides resulting in a change of NDVI mainly where pre-event NDVI is higher due to denser and/or more vigorous vegetation coverage can increase the performance of algorithms ability to identify affected areas (Milledge et al. 2022). Thus, the current study demonstrated that the ability to identify areas with vegetation cover fragility, as observed for NDVI, is only achieved by EVI which seems to be a very close measurement. The MSI, in this turn, evidenced a large spreading of No Vegetation category throughout the basin, which therefore contributed to increase the probability of a match with NDVI, as well as with any other Vi. On the other hand, the VIs also presented high rates of matches for the identification of the categories Intermediate and Vigorous Vegetation, supporting the accuracy of the VIs to diagnostic the healthy state of the vegetation (with exception of MSI), even when the areas presenting these conditions are considered unsatisfactory to ensure no landslide event propensity.

Table 4: Comparison of the accuracy of different VIs with the NDVI (2016) reference

| Category | EVI | GNDVI | RENDVI | VOG1 | ARVI | MSI | NDII | NDWI |
|-------------------------|-----|-------|--------|------|------|-----|------|------|
| No Vegetation | 0% | 13% | 7% | 0% | 0% | 50% | 7% | 7% |
| Declining Vegetation | 75% | 17% | 36% | 15% | 0% | 56% | 50% | 15% |
| Intermediate Vegetation | 89% | 77% | 32% | 47% | 2% | 34% | 72% | 80% |
| Vigorous Vegetation | 47% | 96% | 94% | 92% | 99% | 32% | 15% | 70% |

Thus, the health status of the vegetation cover might be applied to indicate not just the propensity to landslide event, corroborating the statement that most of the landslides might be distributed in areas with a small NDVI, indicating that vegetation coverage had a certain inhibitory effect on landslide occurrence (Zhu et al. 2020). In fact, the state of preservation and the recovering capacity of the vegetation cover on hillside surfaces, which tend to make these areas less susceptible to the landslide event. Therefore, the use of combined VIs presented an acceptable rate of match for all categories, hence highlighting the potential of these indices to differentiate the portion of the vegetation in the higher area of the basin, as well as to distinguish between the different states of vegetation health, and areas with reduced vegetation covering or tending to the bare soil. This statement agrees with the assumption that the combination of different VIs might be recommended to analyze vegetation coverage status in hillslope (Lillesand et al. 2015, Jacquemart and Tiampo 2021), as well as the integration of VIs with abiotic factors might be suitable to the comprehensive understanding of a landslide occurrence (Gomes, et al. 2020, Abeywardana and Gomes 2022). In addition, the modelling of VIs information using deep learning might give new insights onto landslide monitoring by integrating data from different sources of influence (Ferchichi et al. 2022).

The major limitation of the present study was the difficulty in obtaining images, considering the high degree of the slopes and also the occurrence of shaded areas, mainly in those areas facing southwest.

5. Conclusion

The findings suggest that vegetation indexes are suitable for the analysis of areas prone to landslide, highlighting the reliability of VIs to the diagnosis of vegetation classes (i.e., No Vegetation, Declining Vegetation, Intermediate Vegetation, and Vigorous Vegetation) to characterize the major concerns of vegetation state with the ability to increase the propensity to landslide occurrence, such as the reduction of vegetation health status and no vegetation cover. Concomitantly, this study also evidenced that Sentinel-2 image is a confident source of information regarding the vegetation state, therefore enabling affordable image processing for scarped areas. To further improve the quality of vegetation state information on scarped areas, future studies should compare the image processing from orbital sensors with a multispectral sensor coupled to UAV (Unmanned Aerial Vehicles) system, which images are recognized to overcome the constraints (i.e., atmospheric condition and shadowed relief) that affect orbital sensors information. Furthermore, the association between procedures of data acquisition on the changes of vegetation cover and state, and hillside morphology through time have been a tendency to approach the spatiotemporal dynamics from which an accurate feature of the events leading to landslide might be determined. In addition, such as features of vegetation and soil time series data can be modeled with deep learning algorithm to automatize the monitoring of landslide occurrence, and further combined to other influencing factors (e.g., temperature, humidity, and rainfall) to improve the performance of the mapping outcomes.

ACKNOWLEDGEMENT

The authors thank the PETROBRAS (“Meteorological alerts for geological and geotechnical risk assessment in the South and Southeast regions of Brazil”, coordinated by PETROBRAS/CENPES) for scientific support and ANP (National Agency for Petroleum, Natural Gas and Biofuels, Brazil), associated with the investment of resources arising from the Clauses of PD&I. We also thank the National Council for Scientific and Technological Development (CNPq, Brazil 316574/2021-0 to F.A.G.V.R.), for the financial support. And the “Instituto de Geociências e Ciências Exatas - IGCE (Universidade Estadual Paulista – UNESP, Rio Claro) for providing laboratory facilities, especially, to the Research Center in Applied Natural Sciences - UNESPetro and Geology Department (IGCE/UNESP).

AUTHOR’S CONTRIBUTION

Author1: Conceptualization, methodology, drafting (writing – original and review), data collection, data analysis, editing, final approval; Author2: Conceptualization, methodology, drafting (writing – original and review), data collection, data analysis, editing, final approval; Author3: Conceptualization, methodology, drafting (writing – original and review), data curation, data analysis, editing, final approval; Author4: Conceptualization, methodology, drafting (writing – original and review), data collection, data analysis, editing, final approval; Author5: Conceptualization, methodology, drafting (writing – original and review), data curation, data analysis, editing, final approval.

REFERENCES

Abeyisiriwardana, H. D. and Gomes, P. I. A. 2022. Integrating vegetation indices and geo-environmental factors in GISbased landslide-susceptibility mapping: using logistic regression. *Journal of Mountain Science*, 19 (2), pp. 477-492. DOI: 10.1007/s11629-021-6988-8.

- Colwell, J. E. 1974. Vegetation canopy reflectance. *Remote Sensing of Environment*, 3, pp. 175–183. DOI: 10.1016/0034-4257(74)90003-0.
- Corrêa, M. P. and Francelino, M. R. 2015. Avaliação da Influência da Radiação na Regeneração Natural de Mata Atlântica. In: *17th Simpósio Brasileiro de Sensoriamento Remoto*. 25-29 April 2015, João Pessoa: Brazil. pp. 6445-6450.
- Dahigamuwa, T., Yu, Q. and Gunaratne, M. 2016. Feasibility study of land cover classification based on normalized difference vegetation index for landslide risk assessment. *Geosciences*, 6 (4), pp. 45-59. DOI: 10.3390/geosciences6040045.
- Daughtry, C., Walthall, C. L. Kim, M.S., Colstoun E. B. and McMurtrey, J.E. 2000. Estimating Corn Leaf Chlorophyll Concentration from Leaf and Canopy Reflectance. *Remote Sensing Environment*, 74, pp.229-239. DOI: 10.1016/S0034-4257(00)00113-9.
- Debastiani, A. B., Moura, M. M., Rex, F. E., Sanquetta, C. R., Dalla Corte A. P. and Pinto N. 2019. Regressões robusta e linear para estimativa de biomassa via imagem Sentinel em uma floresta tropical. *BIOFIX Scientific Journal*, 4 (2), pp. 81-87. DOI: 10.5380/biofix.v4i2.62922.
- Durante, M., Oesterheld, M., Piñeiro, G. and Vassallo, M. M. 2014. Estimating forage quantity and quality under different stress and senescent biomass conditions via spectral reflectance. *International Journal of Remote Sensing*, 35(9), pp. 2963-2981. DOI: 10.1080/01431161.2014.894658.
- EMBRAPA – Empresa Brasileira de Pesquisa Agropecuária. *Levantamento de reconhecimento dos solos do Estado do Paraná*. Londrina. 1984.
- ESA – Agência Espacial Europeia) *Sentinel-2*. 2018. Available at: <<https://sentinel.esa.int/web/sentinel/missions/sentinel-2>> [Accessed 05 August 2018].
- ESRI – Environmental Systems Research Institute –. *ArcGIS*. 2015. Redlands: ESRI.
- Fan, H. Fu, X. Zhang, Z. and Wu, Q. 2015. Phenology-based vegetation index differencing for mapping of rubber plantations using Landsat OLI data. *Remote Sensing*, 7 (5), pp. 6041-6058. DOI: 10.3390/rs70506041.
- Ferchichi, A., Abbes, A. B., Barra, V. and Farah, I. R. 2022. Forecasting vegetation indices from spatio-temporal remotely sensed data using deep learning-based approaches: A systematic literature review. *Ecological Informatics*, 68, p. 101552. DOI: 10.1016/j.ecoinf.2022.101552.
- Finch, D. A., Bailey, W. G., Mcarthur, L. J. B. and Nasitwitwi, M. 2004. Photosynthetically active radiation regimes in a southern African savana environment. *Agricultural and Forest Meteorology*, 122 (3-4), pp. 229–238. DOI: 10.1016/j.agrformet.2003.09.015.
- Gao, B. 1996. NDWI – A normalized difference water index for remote sensing of vegetation liquid water from space. *Remote Sensing of Environment*, 58 (3), pp. 257-266. DOI: 10.1016/S0034-4257(96)00067-3.
- Gitelson, A., Kaufman, Y. J. and Merzlyak, M. N. 1996. Use of a green channel in remote sensing of global vegetation from EOS-MODIS. *Remote Sensing of Environment*, 58, pp.289-298. DOI: 10.1016/S0034-4257(96)00072-7.
- Gitelson, A. and Merzlyak, M. 1998. Remote Sensing of Chlorophyll Concentration in Higher Plant Leaves. *Advances in Space Research*, 22 (5), pp. 689-692. DOI: 10.1016/S0273-1177(97)01133-2.
- Gomes, P. I., Aththanayake, U., Deng, W., Li, A., Zhao, W. and Jayathilaka, T. 2020. Ecological fragmentation two years after a major landslide: Correlations between vegetation indices and geo-environmental factors. *Ecological Engineering*, 153, p.105914. DOI: 10.1016/j.ecoleng.2020.105914.
- Guidicini, G. and Nieble, C. M. 1984. *Estabilidade de taludes naturais e de escavação*. São Paulo: Edgard Blücher.
- Hardisky, M.A., Klemas, V. and Smart, R. M. 1983. The influences of soil salinity, growth form, and leaf moisture on the spectral reflectance of *Spartina alterniflora* canopies. *Photogrammetric Engineering and Remote Sensing*, 49(1), pp.77-83.
- Horler, D., Dockray, M. and Barber, J. 1983. The red edge of plant leaf reflectance. *International Journal of Remote Sensing*, 4, pp. 273–288. DOI: 10.1080/01431168308948546.

- Hu, J., Ye, B., Bai, Z. and Hui, J. 2022. Comparison of the vegetation index of reclamation mining areas calculated by multi-source remote sensing data. *Land*, 11(3), p. 325. DOI: 10.3390/land11030325.
- Huete, A., Miura, T., Gao, X., Ferreira, L. and Didan, K. 2002. Overview of the Radiometric and Biophysical Performance of the MODIS Vegetation Indices. *Remote Sensing of Environment*, 83, pp. 195-213.
- Hunt, E. R. 1991. Airborne remote sensing of canopy water thickness scaled from leaf spectrometer data. *International Journal of Remote Sensing*, 12, pp. 643-649. DOI: 10.1080/01431169108929679.
- Hunt, E. R., Rock, B. N. and Nobel, P. S. 1987. Measurement of leaf relative water content by infrared reflectance. *Remote Sensing of Environment*, 22, pp. 429-435. DOI: 10.1016/0034-4257(87)90094-0.
- Hunt, E. R. and Rock, B.N. 1989. Detection of changes in leaf water content using near- and middle-infrared reflectances. *Remote Sensing of Environment*, 30 (1), pp.43-54. DOI: 10.1016/0034-4257(89)90046-1.
- 26 Jacquemart, M. and Tiampo, K. 2021. Leveraging time series analysis of radar coherence and normalized difference vegetation index ratios to characterize pre-failure activity of the Mud Creek landslide, California. *Natural Hazards and Earth System Sciences*, 21 (2), pp. 629-642. DOI: 10.5194/nhess-21-629-2021.
- Karsli, F., Atasoy, M., Yalcin, A., Reis, S., Demir, O. N. and Gokceoglu, C. 2009. Effects of land-use changes on landslides in a landslide-prone area (Ardesen, Rize, NE Turkey). *Environmental monitoring and assessment*. 156 (1), pp. 241-255. DOI: 10.1016/0013-7952(92)90053-2.
- Kaufman, Y. J. 1984. Atmospheric effects on remote sensing of surface reflectance. *Remote sensing: critical review of technology*, 475, pp. 20-33. DOI: 10.1117/12.966238.
- Kaufman, Y.J. and Tanre, D. 1992. Atmospherically Resistant Vegetation Index (ARVI) for EOS-MODIS. *IEEE Transactions on Geoscience and Remote Sensing*, 30 (2), pp. 261-270. DOI: 10.1109/36.134076.
- Lillesand, T., Kiefer, R. W. and Chipman, J. 2015. *Remote sensing and image interpretation*. Hoboken: John Wiley & Sons.
- Maack, R. *Geografia Física do Estado do Paraná*. 2.ed. Rio de Janeiro: José Olympio, 1981.
- McFeeters, S. K. 1996. The use of the Normalized Difference Water Index (NDWI) in the delineation of open water features. *International Journal of Remote Sensing*, 17 (7), pp. 1425-1432. DOI: 10.1080/01431169608948714.
- Milledge, D. G., Bellugi, D. G., Watt, J., and Densmore, A. L. 2022. Automated determination of landslide locations after large trigger events: advantages and disadvantages compared to manual mapping. *Natural Hazards and Earth System Sciences*, 22(2), pp. 481-508. DOI: 10.5194/nhess-22-481-2022.
- Meena, S. R., Puliero, S., Bhuyan, K., Floris, M. and Catani, F. 2022. Assessing the importance of conditioning factor selection in landslide susceptibility for the province of Belluno (region of Veneto, northeastern Italy). *Natural hazards and earth system sciences*, 22 (4), pp. 1395-1417. DOI: 10.5194/nhess-22-1395-2022.
- Noda, H. M., Muraoka, H. and Nasahara, K. N. 2021. Plant ecophysiological processes in spectral profiles: perspective from a deciduous broadleaf forest. *Journal of Plant Research*, 134, pp. 737-751. DOI: 10.1007/s10265-021-01302-7.
- Prabhakar, M., Prasad, Y. G. and Rao, M. N. 2012. Remote sensing of biotic stress in crop plants and its applications for pest management. In: B. Venkateswarlu, A. Shanker, C. Shanker and M. Maheswari, eds. 2012. *Crop stress and its management: perspectives and strategies*. pp. 517-545.
- Recanatesi, F., Giuliani, C. and Ripa, M. N. 2018. Monitoring Mediterranean Oak decline in a peri-urban protected area using the NDVI and Sentinel-2 images: the case study of Castelporziano State Natural Reserve. *Sustainability*, 10 (9), pp. 3308. DOI: 10.3390/su10093308.
- Rock, B. N., Vogelmann, J. E., Williams, D. L., Vogelmann, A. F. and Hoshizaki, T. 1986. Remote Detection of Forest Damage: Plant responses to stress may have spectral "signatures" that could be used to map, monitor, and measure forest damage. *Bioscience*, 36 (7), pp. 439-445. DOI: 10.2307/1310339.
- Rouse, J. J. W., Haas, R. H., Deering, D. W. and Schell, J. A. 1973. *Monitoring the Vernal Advancement and Retrogradation (GreenWave Effect) of Natural Vegetation*. Greenbelt: NASA/GSFC.

- Salas, E. A. L. and Henebry, G. M. 2014. A New Approach for the Analysis of Hyperspectral Data: Theory and Sensitivity Analysis of the Moment Distance Method. *Remote Sensing*, 6 (1), pp. 20-41. DOI: 10.3390/rs6010020.
- Schiavo, B. N. V. 2016. *Métodos para estimativa do índice de área foliar em um fragmento de floresta ombrófila mista montana no Estado do Paraná*. MSc. – Federal University of Parana.
- Segoni, S., Piciullo, L. and Gariano, S. L. 2018. A review of the recent literature on rainfall thresholds for landslide occurrence. *Landslides*, 15, pp. 1483–1501. DOI: 10.1007/s10346-018-0966-4.
- Shen, P., Zhang, L. M., Fan, R. L., Zhu, H. and Zhang, S. 2020. Declining geohazard activity with vegetation recovery during first ten years after the 2008 Wenchuan earthquake. *Geomorphology*, 352, 106989. DOI: 10.1016/j.geomorph.2019.106989.
- Sims, D. A. and Gamon, J. A. 2002. Relationships Between Leaf Pigment Content and Spectral Reflectance Across a Wide Range of Species, Leaf Structures and Developmental Stages. *Remote Sensing of Environment*, 81, pp. 337-354. DOI: 10.1016/S0034-4257(02)00010-X.
- Vanhellemont, Q. and Ruddick, K. 2016. Acolite for Sentinel-2: Aquatic applications of MSI imagery. In: *Proceedings of the 2016 ESA Living Planet Symposium, 2016 Prague*. pp. 9-13.
- Veloso, H.P., Rangel Filho, A.L. and Lima, J.C. 1991. *Classificação da Vegetação brasileira adaptada a um sistema universal*. IBGE-Departamento de Recursos Naturais e Estudos Ambientais. Rio de Janeiro, 1991.
- Vogelmann, T. 1993. Plant tissue optics. *Annual Review of Plant Physiology and Plant Molecular Biology*, 44, pp. 231–251. DOI: 10.1146/annurev.arplant.44.1.231.
- Vogelmann, J. E., Rock, B. N. and Moss, D. M. 1993. Red Edge Spectral Measurements from Sugar Maple Leaves. *International Journal of Remote Sensing*, 14 (8), pp. 1563-1575. DOI: 10.1080/01431169308953986.
- Wolle, C. M. and Carvalho, C. S. 1989. Deslizamentos em encostas na Serra do Mar - Brasil. *Solos e Rochas*, São Paulo, 12, pp. 27-36.
- Yi, Y., Zhang, Z., Zhang, W., Xu, Q., Deng, C. and Li, Q. 2019. GIS-based earthquake-triggered-landslide susceptibility mapping with an integrated weighted index model in Jiuzhaigou region of Sichuan Province, China. *Natural Hazards and Earth System Sciences*, 19 (9), pp. 1973–1988. DOI: 10.5194/nhess-19-1973-2019.
- Zhang, S., Zhang, L. M. and Glade, T. 2014. Characteristics of earthquake and rain-induced landslides near the epicenter of Wenchuan earthquake. *Engineering Geology*, 175, pp. 57-73. DOI: 10.1016/j.enggeo.2014.03.012.
- Zhu, L., Huang, L., Fan, L., Huang, J., Huang, F., Chen, J., Zhang, Z. and Wang, Y. 2020. Landslide susceptibility prediction modeling based on remote sensing and a novel deep learning algorithm of a cascade-parallel recurrent neural network. *Sensors*, 20(6), 1576. DOI: 10.3390/s20061576.
- Zou, Y., Chen, W., Li, S.; Wang, T., Yu, L., Xu, M., Singh, R. P. and Liu, C. Q. 2022. Spatio-Temporal Changes in Vegetation in the Last Two Decades (2001–2020) in the Beijing–Tianjin–Hebei Region. *Remote Sensing*, 14 (16), p. 3958. DOI: 10.3390/rs14163958.